Tunneling Under Interference with Reconfigurable Intelligent Surfaces

Eyad Shtaiwi, *Member IEEE*, George Sklivanitis, *Member IEEE*, Dimitris A. Pados *Senior Member IEEE*, and Elizabeth Serena Bentley, *Member IEEE*

***Abstract*—Reconfigurable intelligent surface (RIS) technology is gaining significant attention from academia and industry due to its potential to greatly enhance coverage, spectral and energy efficiency, and security in next-generation (NextG) wireless communication systems. In this paper, we present a novel framework to avoid interference near a NextG receiver with the installation of an RIS. In particular, first we minimize the smallest eigenvalue of the locally-sensed interference-plus-noise covariance matrix (INCM) by optimizing phase shifts of the RIS to open a new "clean" eigen-mode of communication. Then, we carry out optimal design of a multiple-input multiple-output (MIMO) transmit waveform that takes advantage of the reconfigured wireless environment around the receiver and maximizes the pre-detection signal-to-interference-plus-noise ratio (SINR). Extensive simulation studies included in this paper illustrate our theoretical developments and show that phase optimizing an RIS near the receiver can reduce the smallest eigenvalue of INCM by up to 90% or more leading to remarkably enhanced pre-detection SINR by subsequently optimized MIMO waveforms.**

***Index Terms*—Interference alignment, interference avoidance, reconfigurable intelligent surfaces (RIS), manifold optimization, MIMO, spectrum sharing, waveform design.**

I. Introduction

Reconfigurable intelligent surfaces (RIS) have recently attracted widespread interest as enabling technology for next-generation (NextG) networks. Use of optimized RIS may enhance the presence of signals of interest and/or suppress interference. Early work on spectrum sharing with RIS was reported in [1]. Recent work on RIS-enabled interference mitigation includes [2], [3] and references therein, as well as [4] where the authors considered multicast communications. Characterization of information-theoretic capacity in RIS-equipped interference environments was carried out in [5].

Further studies considered RIS-assisted sum rate maximization in multi-user multiple-input single-output (MISO) systems [6] and interference alignment in multiple-input multiple-output device-to-device (MIMO D2D) networks by jointly optimizing beamforming, precoding, and RIS phase shifts to improve signal-to-interference-plus-noise ratio (SINR) and overall network performance [7]. The effect of imperfect channel state information (CSI) and hardware impairments in RIS wireless communication systems was examined in [8], [9] in terms of achievable data rate, outage probability, and bit error rate. In [10], [11], the authors suggested a novel use of RIS for signal cancellation to address the challenge of radio frequency interference (RFI) in Radio Astronomy Services (RAS). Before the interference reaches the analog-to-digital converter, it is canceled by an RIS that generates a destructive wavefront at the radio telescope [10] by controlling the RIS phase and amplitude parameters [11]. RIS phase adaptation can be effectively driven by tailored manifold optimization procedures such as the unified manifold optimization framework to maximize spectral efficiency of RIS-aided point-to-point MIMO communication system in [12] or the Riemannian manifold optimizer in [13] to enhance the achievable sum-secrecy-rate of RIS-assisted integrated sensing and communication systems. In terms of performance analysis of RIS-aided MIMO communications, recent works in the literature include [14] that examined base-to-users downlink transmissions with or without a direct (i.e., non-RIS) channel and [15] that derived closed-form expressions for the spatially ergodic rate in multi-RIS-aided networks.

To the best knowledge of the authors, no existing work to date addresses the potential of RIS technology to enable and sustain a new MIMO link over a heavily congested frequency band [16], [17]. In this paper, for the first time in the literature, we design dynamically maximum pre-detection SINR MIMO transceivers in arbitrary dense interference environments by utilizing RIS technology to tunnel through disturbances at a given receiver (Rx) location. The novel technical contributions in this paper are as follows.

- We formulate and solve a minimization problem for the smallest eigenvalue of the receiver sensed joint-space-time interference-plus-noise covariance matrix (INCM) as influenced by disturbance sources and a locally placed phase-adjustable RIS. We model the unity modulus of the RIS phase shifts as a Cartesian product of complex unit circle manifolds and leverage the Riemannian Conjugate Gradient method [18] to optimally design the RIS phase values to minimize the smallest eigenvalue of INCM.
- Having opened an effective "eigen-mode" of communication with the RIS through potentially heavy interference, we next find the jointly optimal transmit beam weight vector and coded time-domain waveform to create a max-SINR MIMO link in the space-time domain.

We carry out extensive simulation studies to evaluate the proposed framework in varying interference scenarios. The studies demonstrate that RIS may reduce the smallest eigenvalue of the INCM by as much as 250% and provide $10dB$ gain in SINR compared to max-SINR optimal MIMO without RIS.

Notation: In the following, matrices are denoted by upper-case bold letters, column vectors by lower-case bold letters, and scalars by lower-case plain-font letters. The transpose

This work was supported in part by NSF Grants EEC-2133516 and CNS-2117822, and by the Air Force Research Laboratory Grant FA8750-21-F-1012.

Eyad Shtaiwi, George Sklivanitis, and Dimitris A. Pados are with the Center for Connected Autonomy and AI and the EECS Dept., Florida Atlantic University, Boca Raton, FL 33431 USA (e-mail: {eshtaiwi, gsklivanitis, dpados}@fau.edu). E. S. Bentley is with the Air Force Research Laboratory, AFRL/RI, Rome, NY 13441 USA (e-mail: elizabeth.bentley.3@us.af.mil).

Distribution A. Approved for public release: Distribution Unlimited: AFRL-2025-0652 on 06 Feb 2025.

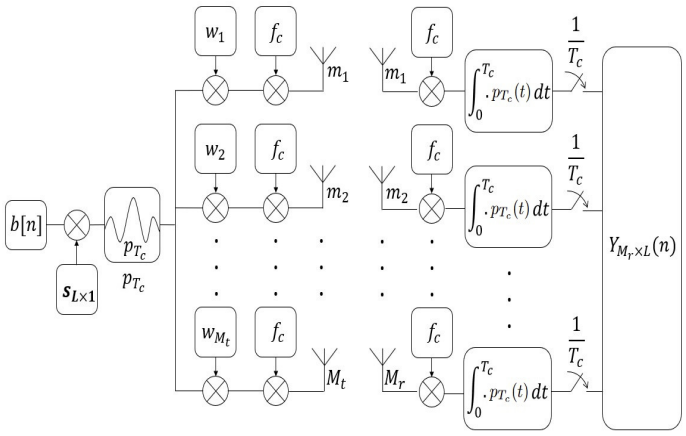

Fig. 1: MIMO system model [16].

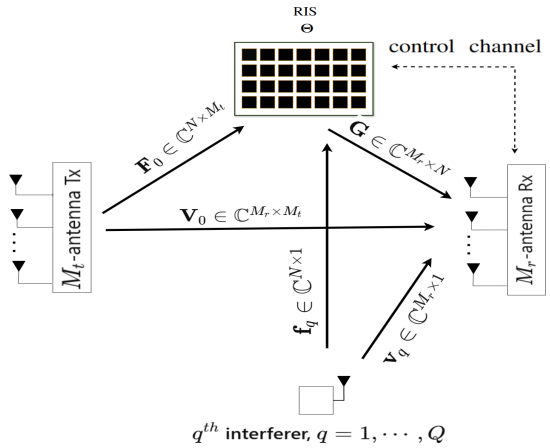

Fig. 2: RIS-assisted MIMO system in the presence of multiple interfering sources.

operation is represented by the superscript ^{T}, conjugation by *, the Hermitian operation (conjugate transpose) by ^{H}, the Kronecker product by $\otimes$, and the outer product by $\odot$.

II. System Model and Notation

We consider a MIMO link of M_t transmit and M_r receive antennas as seen in Fig. 1 that may be assisted by a locally installed RIS module as seen in Fig. 2. The spectral environment includes single-antenna interferers $q \in \{1, \ldots, Q\}$ contributing to in-band disturbance sensed by the receiving node Rx. The RIS module consists of N elements. In this paper, we adopt the ideal phase-shift model under which the operation of the RIS reflecting elements is described by the diagonal matrix $\mathbf{\Theta} \triangleq \text{diag}\left(\mathrm{e}^{j\vartheta_1}, \mathrm{e}^{j\vartheta_2}, \cdots, \mathrm{e}^{j\vartheta_N}\right)$ where $\vartheta_i \in [0, 2\pi)$ represents the phase shift of RIS element $i = 1, 2, \ldots, N$ [19]. As seen in Fig. 2, $\mathbf{G} \in \mathbb{C}^{M_r\times N}$ represents the channel matrix between RIS and Rx, while the matrices $\mathbf{V}_0 \in \mathbb{C}^{M_r\times M_t}$ and $\mathbf{F}_0 \in \mathbb{C}^{N\times M_t}$ represent the channel between transmitter Tx and Rx and Tx and RIS, respectively. Furthermore, $\mathbf{v}_q \in \mathbb{C}^{M_r\times 1}$ and $\mathbf{f}_q \in \mathbb{C}^{N\times 1}$ denote the energy-inclusive channel vector from the qth interferer to Rx and RIS, respectively, $q = 1, \ldots, Q$. All channel realizations are assumed to remain constant during the RIS and MIMO link adaptation process described in the sequel.

The combined effective channel between the qth interferer and Rx is denoted by $\mathbf{h}_q$ and can be expressed as

$$\begin{aligned}\mathbf{h}_q &= \mathbf{G}\,\text{diag}\,(\boldsymbol{\theta})\,\mathbf{f}_q + \mathbf{v}_q = \mathbf{G}\,\text{diag}\,(\mathbf{f}_q)\,\boldsymbol{\theta} + \mathbf{v}_q \\ &= \mathbf{A}_q\boldsymbol{\theta} + \mathbf{v}_q \end{aligned} \tag{1}$$

where $\mathbf{A}_q \triangleq \mathbf{G}\,\text{diag}\,(\mathbf{f}_q)$ and $\boldsymbol{\theta} \triangleq \left[\mathrm{e}^{j\vartheta_1}, \mathrm{e}^{j\vartheta_2}, \cdots, \mathrm{e}^{j\vartheta_N}\right]^T$. Similarly, the combined effective end-to-end channel between Tx and Rx [23] denoted by $\mathbf{H}_{\text{eff}}$ is given by

$$\mathbf{H}_{\text{eff}} = \mathbf{G}\,\text{diag}\,(\boldsymbol{\theta})\,\mathbf{F}_0 + \mathbf{V}_0 \in \mathcal{C}^{M_r\times M_t}. \tag{2}$$

Without loss of generality, we assume (see Fig. 1) that Tx transmits a bit sequence $b(n) \in \{\pm 1\}$, $n = 0, 1, \ldots, N_b$, at rate $1/T_b$ across all antennas on carrier frequency f_c using a time-domain code-shaped waveform $s(t)$ of duration T_b,

$$s(t) = \sum_{l=0}^{L-1} s(l) p_{T_c}\left(t - lT_c\right) \tag{3}$$

where $\mathbf{s}(l) \in \{\pm 1/\sqrt{L}\}$ denotes the lth bit of the waveform code vector $\mathbf{s}_{L\times 1}$ and $p_{T_c}(\cdot)$ is a square-root raised cosine (SRRC) pulse with duration $T_c = T_b/L$. Each pulse is normalized to unit energy, i.e., $\int_0^{T_c} |p_{T_c}(t)|^2\,dt = 1$. The signal transmitted by the ith Tx antenna $v_i(t)$, $i = 1, \ldots, M_t$, is

$$v_i(t) = \sqrt{E_b} \sum_{n=0}^{N_b-1} b(n) s(t - nT_b) e^{j2\pi f_c t} w_i \tag{4}$$

where $E_b > 0$ is the transmitted energy per bit per antenna and $w_i \in \mathbb{C}$ is the antenna beam weight value.

The received signal at node Rx after carrier demodulation across antennas has the vector form

$$\mathbf{r}_{M_r\times 1}(t) = \sqrt{E_b} \sum_{n=0}^{N_b-1} b(n) s(t - nT_b) \mathbf{H}_{\text{eff}} \mathbf{w}_{M_t} + \mathbf{i}(t) + \mathbf{n}(t) \tag{5}$$

where $\mathbf{w}_{M_t} = [w_1 \cdots w_{M_t}]^T$ is the Tx beam weight vector, and $\mathbf{i}(t) \in \mathbb{C}^{M_r\times 1}$, $\mathbf{n}(t) \in \mathbb{C}^{M_r\times 1}$ model comprehensively overall locally-sensed post-carrier-demodulation environmental disturbance and additive white Gaussian noise, respectively.

Upon pulse-matched filtering at each Rx antenna over L successive pulses during bit period n, $n = 1, 2, \cdots, N_b$, the collected data are organized in the form of the space-time matrix $\mathbf{Y}_{M_r\times L}(n)$, which can be vectorized to

$$\begin{aligned}\mathbf{y}_{M_rL\times 1}(n) &= \text{vec}\{\mathbf{Y}_{M_r\times L}(n)\} \\ &= \sqrt{E}\, b(n)(\mathbf{s} \otimes \mathbf{H}_{\text{eff}})\mathbf{w}_{M_t} + \mathbf{i}(n) + \mathbf{n}(n) \end{aligned} \tag{6}$$

where $\mathbf{i}(n)$ and $\mathbf{n}(n)$ represent post-matched-filtered interference and white noise in the space-time receiver domain.

With the RIS set at an arbitrary phase configuration $\boldsymbol{\theta}$ and stationary interference signaling across time, the compound space-time disturbance $\mathbf{i}(n) + \mathbf{n}(n) \in \mathbb{C}^{M_rL}$ has autocovariance matrix (INCM)

$$\tilde{\mathbf{R}}_{i+n} \triangleq E\left\{\left(\mathbf{i}(n) + \mathbf{n}(n)\right)\left(\mathbf{i}(n) + \mathbf{n}(n)\right)^H\right\} = \mathbf{1}_L\mathbf{1}_L^T \otimes \mathbf{R}_{i+n} \tag{7}$$

where $\mathbf{1}_L$ is the all-one vector of length L and $\mathbf{R}_{i+n} \in \mathbb{C}^{M_r \times M_r}$ is the space-domain INCM given by

$$\mathbf{R}_{i+n} = \sum_{q=1}^{Q} \left(\mathbf{A}_q \boldsymbol{\theta} \boldsymbol{\theta}^H \mathbf{A}_q^H + \mathbf{A}_q \boldsymbol{\theta} \mathbf{v}_q^H + \mathbf{v}_q \boldsymbol{\theta}^H \mathbf{A}_q^H \right) + \mathbf{R}_{i+n}^{off} \tag{8}$$

with $\mathbf{R}_{i+n}^{off}$ representing INCM in the absence of the RIS. Since $\mathbf{1}_L \mathbf{1}_L^T$ has only one eigenvalue ($\mu_1 = L$), the eigenvectors of $\mathbf{R}_{i+n}$ in (8) represent the space-time directions in which the receiver detects interference with the corresponding eigenvalues indicating interference power (variance). When the eigenvalues are sorted in descending order, the direction with the least interference is defined by the eigenvector associated with the smallest eigenvalue.

III. RIS Optimization

We are interested in minimizing the smallest eigenvalue of the INCM in (8) by adjusting the RIS phase shifts in $\boldsymbol{\theta} = \left[\mathrm{e}^{j\vartheta_1}, \mathrm{e}^{j\vartheta_2}, \cdots, \mathrm{e}^{j\vartheta_N} \right]^T$. The optimization problem is formulated as follows:

$$\boldsymbol{\theta}^o = \underset{\boldsymbol{\theta}}{\operatorname{argmin}} \ \lambda_{\min}(\mathbf{R}_{i+n}) \tag{9a}$$

$$\text{subject to } |\theta_i| = 1, \ i = 1, 2, \cdots, N, \tag{9b}$$

where $\lambda_{\min}$ represents the smallest eigenvalue of $\mathbf{R}_{i+n} \in \mathbb{C}^{M_r \times M_r}$ in (8). The constraint in (9b) enforces a constant modulus per coordinate introducing non-convexity to the optimization problem. The smallest eigenvalue of $\mathbf{R}_{i+n}$ is equal to the reciprocal of the maximum eigenvalue of its inverse. Therefore, (9a) can be rewritten as

$$\boldsymbol{\theta}^o = \underset{\boldsymbol{\theta}}{\operatorname{argmin}} \ \lambda_{\max}^{-1}(\mathbf{R}_{i+n}^{-1}), \tag{10a}$$

$$\text{subject to } |\theta_i| = 1, \ i = 1, 2, \cdots, N. \tag{10b}$$

$\mathbf{R}_{i+n}^{-1}$ is positive semi-definite meaning that its maximum eigenvalue can be well approximated by the scaled Frobenius norm, i.e., $\lambda_{\max}(\mathbf{R}_{i+n}^{-1}) \approx \frac{\|\mathbf{R}_{i+n}^{-1}\|_F}{\sqrt{M_r L}}$ [20, Th. 5.6.9]. Then, the optimization problem can be reformulated approximately as

$$\boldsymbol{\theta}^o = \underset{\boldsymbol{\theta}}{\operatorname{argmin}} f(\boldsymbol{\theta}) \triangleq \|\mathbf{R}_{i+n}^{-1}\|_F^{-1} \tag{11a}$$

$$\text{subject to } |\theta_i| = 1, \ i = 1, 2, \cdots, N. \tag{11b}$$

The constant-modulus constraint (CMC) in (11b) restricts the search space to a smooth Riemannian complex-circle manifold (CCM) embedded in $\mathbb{C}^N$,

$$\mathcal{M}^N \triangleq \{\boldsymbol{\theta} \in \mathbb{C}^N : \theta_i^* \theta_i = 1, \ i = 1, 2, \ldots, N\}. \tag{12}$$

Optimization on manifolds has been widely studied in the recent past, offering reduced computational cost and high-quality solutions for NP-hard problems [21]. In this paper, we propose to use alternating manifold optimization on $\mathcal{M}^N$ to address (11a), (11b) in the unconstrained form

$$\boldsymbol{\theta}^o = \underset{\boldsymbol{\theta} \in \mathcal{M}^N}{\operatorname{argmin}} f(\boldsymbol{\theta}). \tag{13}$$

We solve (13) by gradient descent (GD) on the CCM executed in three steps: (i) Compute the Riemannian gradient; (ii) descent within the tangent space; and (iii) map back to CCM, all repeated until a stopping criterion is met.

1) Gradient Projection: The Riemannian gradient of the objective function $f(\boldsymbol{\theta})$ in (13) at point $\boldsymbol{\theta}_k \in \mathcal{S} \triangleq \mathcal{M}^N$ is denoted by $\nabla_{\mathcal{S}} f(\boldsymbol{\theta}_k)$ and computed by projecting the Euclidean gradient onto the tangent space. Hence, at iteration point $\boldsymbol{\theta}_{(i)}$

$$\begin{aligned} \nabla_{\mathcal{S}} f\left(\boldsymbol{\theta}_{(i)}\right) =& \mathbf{P}_{\mathcal{T}_{\boldsymbol{\theta}_{(i)}}\mathcal{S}} \left(\nabla_{\boldsymbol{\theta}} f\left(\boldsymbol{\theta}_{(i)}\right) \right) \\ =& \nabla_{\boldsymbol{\theta}} f\left(\boldsymbol{\theta}_{(i)}\right) - \Re\left\{ \nabla_{\boldsymbol{\theta}} f\left(\boldsymbol{\theta}_{(i)}\right) \odot \boldsymbol{\theta}_{(i)}^* \right\} \odot \boldsymbol{\theta}_{(i)} \end{aligned} \tag{14}$$

where $T_{\boldsymbol{\theta}_{(i)}}\mathcal{S}$ is the space of all tangent vectors $\boldsymbol{\omega}$ at point $\boldsymbol{\theta}_{(i)}$ of $\mathcal{S}$, $T_{\boldsymbol{\theta}_{(i)}}\mathcal{S} \triangleq \left\{ \boldsymbol{\omega} \in \mathcal{C}^N : \Re\left(\boldsymbol{\omega} \odot \boldsymbol{\theta}_{(i)}^* \right) = \mathbf{0}_N \right\}$, where $\Re(\bullet)$ denotes the real part of a complex vector and $\odot$ represents element-wise multiplication, $\mathbf{P}_{\mathcal{T}_{\boldsymbol{\theta}_i}\mathcal{M}}(\bullet)$ is the projection operator from the Riemannian space onto the tangent space, and $\nabla_{\boldsymbol{\theta}} f\left(\boldsymbol{\theta}_{(i)}\right)$ is the Euclidean gradient of (13) at point $\boldsymbol{\theta}_{(i)}$ given by

$$\begin{aligned} &\nabla_{\boldsymbol{\theta}} f\left(\boldsymbol{\theta}_{(i)}\right) = \\ &\frac{2\sqrt{M_r L}}{\|\mathbf{R}_{\mathbf{i+n}}^{-1}\|_F} \left(\sum_{q=1}^{Q} \mathbf{A}_q^H (\mathbf{R}_{\mathbf{i+n}}^{-1})^3 \mathbf{A}_q \boldsymbol{\theta}_{(i)} + \sum_{q=1}^{Q} \mathbf{A}_q^H (\mathbf{R}_{\mathbf{i+n}}^{-1})^3 \mathbf{v}_q \right). \end{aligned} \tag{15}$$

2) Steepest-Descent on $T_{\boldsymbol{\theta}_{(i)}}\mathcal{S}$: Solution updates are created iteratively by

$$\boldsymbol{\theta}_{(i+1)} = \boldsymbol{\theta}_{(i)} - \beta \ \mathbf{P}_{\mathcal{T}_{\boldsymbol{\theta}_{(i)}}\mathcal{M}}(\nabla_{\boldsymbol{\theta}} f(\boldsymbol{\theta}_{(i)})) \tag{16}$$

where $\boldsymbol{\theta}_{(i)} = \left[e^{j\vartheta_1(i)}, e^{j\vartheta_2(i)}, \cdots, e^{j\vartheta_N(i)} \right]^T$, $\beta \in \mathbb{R}^+$ is the step size, and $\mathbf{P}_{\mathcal{T}_{\boldsymbol{\theta}_{(i)}}\mathcal{M}}(\nabla_{\boldsymbol{\theta}} f(\boldsymbol{\theta}_{(i)}))$ is the search direction.

3) Retraction: The updated value does not necessarily lie on the manifold surface. The retraction operator provides an updated feasible solution by "correcting" $\boldsymbol{\theta}_{(i+1)}$ to

$$\begin{aligned} &\boldsymbol{\theta}_{(i+1)} := \boldsymbol{\theta}_{(i+1)} \odot \\ &\left[|\theta_{(i+1)}(1)|^{-1}, |\theta_{(i+1)}(2)|^{-1}, \cdots, |\theta_{(i+1)}(N)|^{-1} \right]^T \end{aligned} \tag{17}$$

by element-by-element normalization.

The optimization procedure is tabulated for easy reference as Algorithm 1. The updated solution in (16) from Step 2 of the algorithm will produce a point on the tangent space $T_{\boldsymbol{\theta}_{(i)}}\mathcal{S}$ and reduce the cost function if the step size β is properly chosen. A condition on the step size that ensures reduction in the cost function is $0 < \beta < \frac{2}{\zeta}$ where ζ is the Lipschitz constant which bounds all eigenvalues of the Hessian matrix $\nabla_{\boldsymbol{\theta}}^2 f\left(\boldsymbol{\theta}_{(i)}\right)$. Under the Lipschitz constant condition, convergence of the proposed method is guaranteed.

Computation of the gradients in (15) and their projections onto the tangent spaces of the complex circle manifold determine the complexity of the overall algorithm. The total complexity of each iteration in the proposed approach is $O((M_r L)^3 + Q M_r^2 L^2 + M_t M_r L + Q M_r N)$.

IV. Link Optimization

Upon adjusting the RIS by Algorithm 1, the next step is to create an optimal (maximum pre-detection SINR) link taking advantage of the communication eigen-mode that was opened

This article has been accepted for publication in IEEE Wireless Communications Letters. This is the author's version which has not been fully edited and content may change prior to final publication. Citation information: DOI 10.1109/LWC.2025.3568636

Algorithm 1 RIS Phase Shifts Optimization

Initialization: $i = 0$; $\boldsymbol{\theta}_{(0)} \in \mathcal{S} \triangleq \mathcal{M}^N$ manifold; $\epsilon > 0$;
while $\|\nabla_{\mathcal{S}} f(\boldsymbol{\theta}_i)\| > \epsilon$ **do**
  Compute Euclidean gradient $\nabla_{\boldsymbol{\theta}} f\left(\boldsymbol{\theta}_{(i)}\right)$ by (15) ;
  Compute Reimannian gradient $\nabla_{\mathcal{S}} f\left(\boldsymbol{\theta}_{(i)}\right)$ by (14) ;
  Update point to $\boldsymbol{\theta}_{(i+1)}$ by (16) and retract by (17) ;
  $i = i + 1$
end
return $\boldsymbol{\theta}^o$

up by the optimized RIS. Building on our previous work [16], [17], we design the transmit beam weight vector $\mathbf{w}_{M_t}$ and time-domain code vector $\mathbf{s}$ to maximize the pre-detection SINR at the receiving node Rx (Figs. 1, 2). The space-time matched-filter is [16]

$$\mathbf{w}_{\text{MF}} \triangleq E\left\{\mathbf{y}_{M_r L\times 1}(n)\; b(n)\right\} = (\mathbf{s}\otimes \mathbf{H}_{\text{eff}})\mathbf{w}_{M_t} \tag{18}$$

and the space-time maxSINR receiver filter is computed by

$$\mathbf{w}_{\text{maxSINR}} = k\,\mathbf{R}_{i+n}^{-1}(\boldsymbol{\theta}^o)(\mathbf{s}\otimes \mathbf{H}_{\text{eff}})\mathbf{w}_{M_t},\; k\in\mathbb{C}. \tag{19}$$

Then, the output SINR of the maxSINR space-time filter is

$$\begin{aligned}&\text{SINR}(\mathbf{s},\mathbf{w}_{M_t})\\ &\triangleq \frac{\text{E}\left\{\left|\mathbf{w}_{\text{maxSINR}}^H\left(\sqrt{E_t}b(n)(\mathbf{s}\otimes \mathbf{H}_{\text{eff}})\mathbf{w}_{M_t}\right)\right|^2\right\}}{\text{E}\left\{\left|\mathbf{w}_{\text{maxSINR}}^H\left(\mathbf{i}(n)+\mathbf{n}(n)\right)\right|^2\right\}}\\ &= E_t\left[(\mathbf{s}\otimes \mathbf{H}_{\text{eff}})\mathbf{w}_{M_t}\right]^H\mathbf{R}_{i+n}^{-1}(\boldsymbol{\theta}^o)(\mathbf{s}\otimes \mathbf{H}_{\text{eff}})\mathbf{w}_{M_t}\end{aligned} \tag{20}$$

which depends on the transmit beam weight vector $\mathbf{w}_{Mt}$ and time-domain code vector $\mathbf{s}$. We aim to determine the optimal $\mathbf{w}_{Mt}$ and $\mathbf{s}$ that maximize SINR for the given RIS-modified disturbance autocorrelation matrix.

If $\mathbf{u}_{\max}$ is the eigenvector of $\mathbf{R}_{i+n}^{-1}(\boldsymbol{\theta}^o)$ with highest eigenvalue, then $\text{SINR}(\mathbf{s},\mathbf{w}_{M_t})$ in (20) is maximized when $(\mathbf{s}\otimes \mathbf{H}_{\text{eff}})\mathbf{w}_{M_t}$ becomes equal to $\mathbf{u}_{\max}$. We put forward, therefore, the following optimization problem,

$$(\mathbf{s}^o,\mathbf{w}_{M_t}^o) = \underset{\mathbf{s}\in\{\pm 1/\sqrt{L}\}^L,\mathbf{w}_{M_t}\in\mathbb{C}^{M_t}}{\text{argmin}} ||(\mathbf{s}\otimes \mathbf{H}_{\text{eff}})\mathbf{w}_{M_t} - \mathbf{u}_{\max}||^2, \tag{21}$$

which has a closed-form solution for the beam weight vector

$$\mathbf{w}_{M_t}^o = [(\mathbf{s}^T\otimes \mathbf{H}_{\text{eff}}^H)(\mathbf{s}\otimes \mathbf{H}_{\text{eff}})]^{-1}(\mathbf{s}^T\otimes \mathbf{H}_{\text{eff}}^H)\mathbf{u}_{\max} \tag{22}$$

for any given code vector $\mathbf{s}$. Inserting (22) in (20), we can find the jointly optimal code vector $\mathbf{s}^o$ with binary search

$$\mathbf{s}^o = \underset{\mathbf{s}\in\{\pm 1/\sqrt{L}\}^L}{\text{argmax}} \left[(\mathbf{s}\otimes \mathbf{H}_{\text{eff}})\mathbf{w}_{M_t}^o\right]^H\mathbf{R}_{i+n}^{-1}(\boldsymbol{\theta}^o)(\mathbf{s}\otimes \mathbf{H}_{\text{eff}})\mathbf{w}_{M_t}^o. \tag{23}$$

V. Simulation Studies

We carry out extensive Monte Carlo simulations to validate the effectiveness of the proposed interference avoidance framework using RIS. Performance is assessed under "moderate" and "dense" interference conditions. In the moderate interference scenario, the number of single-antenna interfering transmitters is set to $Q = M_r$ with transmit energy per bit-over-N_0 for each interferer set to $10dB$, where $N_0/2$ characterizes the white Gaussian noise power spectral density. In the dense interference scenario, $Q = 10M_r$ and the transmit energy per bit-over-N_0 of each interferer is $15dB$. The Tx MIMO link to be optimized is set at $M_t = 4$ with waveform codelength $L = 4$. The size of the RIS is set to $N = 32$. Channel matrices/vectors are generated element-by-element independently as complex Gaussian $\mathcal{N}(0,\sigma^2 = 1)$. All results are averages over $1,000$ independent realizations.

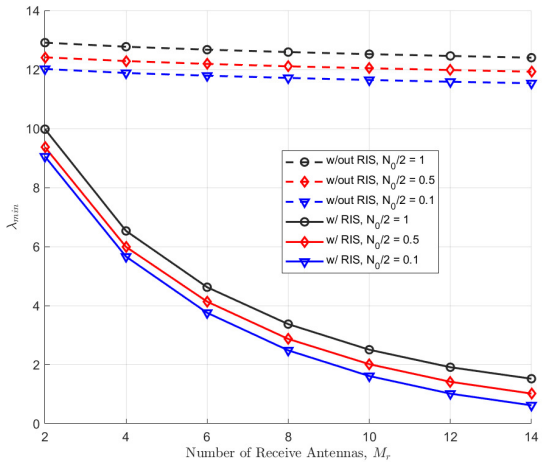

Fig. 3: Smallest eigenvalue of $\mathbf{R}_{i+n}$ in moderate interference.

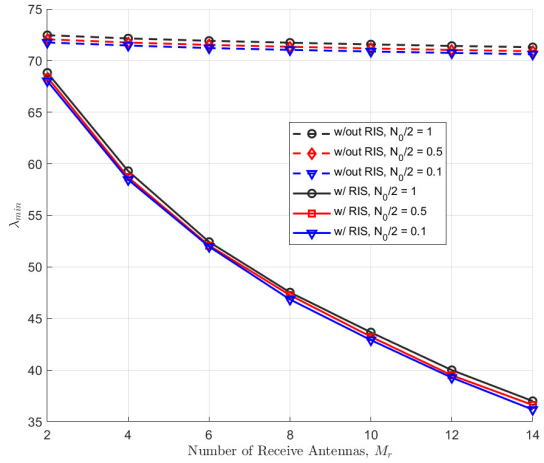

Fig. 4: Smallest eigenvalue of $\mathbf{R}_{i+n}$ in dense interference.

Fig. 3 showcases the role of RIS in minimizing the smallest eigenvalue $\lambda_{\min}$ of INCM under moderate interference and white Gaussian noise of nominal power spectral density $N_0/2$ equal to 1, 0.5, or 0.1. The optimized RIS brings down significantly the smallest eigenvalue of INCM close to the white noise power spectral density value for $M_r = 14$. Fig. 4 repeats the same study in the dense interference scenario. While the optimized RIS does not reduce $\lambda_{\min}$ down to the white noise power spectral density value, it does manage to cut its value in half for $M_r = 14$.

Upon RIS optimization by Algorithm 1, in Fig. 5 we study the pre-detection SINR of an optimized MIMO waveform by (22), (23) that operates under moderate interference with $M_r = 4$ receive antennas. We compare against a similarly optimized MIMO waveform without RIS and an arbitrary

This article has been accepted for publication in IEEE Wireless Communications Letters. This is the author's version which has not been fully edited and content may change prior to final publication. Citation information: DOI 10.1109/LWC.2025.3568636

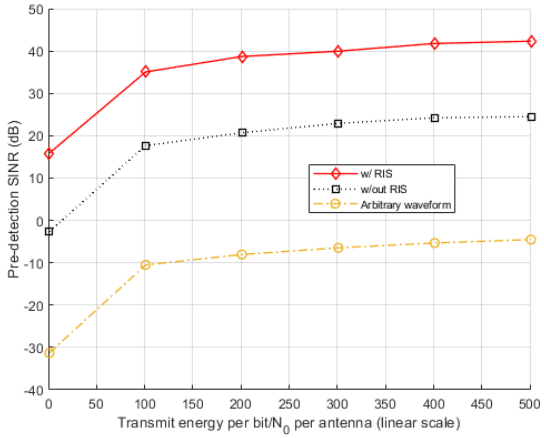

Fig. 5: Pre-detection SINR in moderate interference.

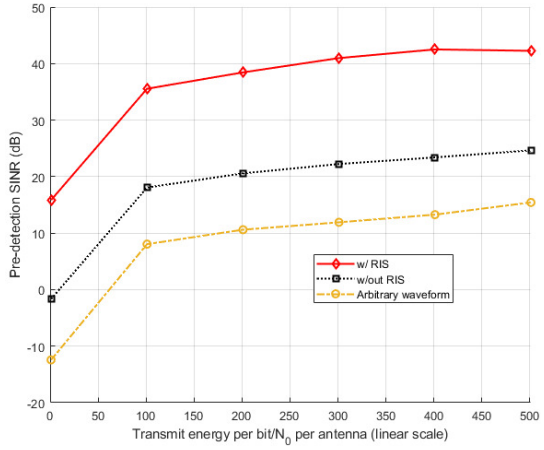

Fig. 6: Pre-detection SINR in dense interference.

MIMO waveform without RIS, but still employing joint space-time maximum SINR pre-detection filtering. Waveform optimization alone adds about $10dB$ in SINR over the arbitrary waveform. Remarkably, when waveform optimization is preceded by RIS optimization an additional gain of about $19dB$ is added on top. Highly reliable, high data-rate transmission is then possible at minimal transmit energy per bit-over-N_0 (e.g., 64-QAM supported by $15dB$ pre-detection SINR).

Fig. 6 repeats the same study for dense interference with practically identical link optimization findings. Notably, arbitrary waveform design with optimal space-time maximum SINR receiver filtering never reaches $0dB$ pre-detection SINR.

VI. Conclusion

We presented a new powerful method to introduce and sustain MIMO links in potentially heavily occupied frequency bands with the use of a phase-adjustable RIS placed near the receiving node. In particular, we formulated and solved an RIS optimization problem to minimize the smallest eigenvalue of the disturbance (interference-plus-noise) space-time autocovariance matrix at the receiver. Successful minimization of the smallest disturbance eigenvalue opens up the corresponding eigen-mode for MIMO communication. The available eigen-mode is then found dynamically by transmit beam weight vector and coded time-domain signal optimization.

Future work may pursue joint RIS and MIMO waveform optimization, as well as multi-user/multi-receiver networks.

References

[1] X. Tan, Z. Sun, J. M. Jornet, and D. A. Pados, "Increasing indoor spectrum sharing capacity using smart reflect-array," in *Proc. IEEE Int. Conf. Commun. (ICC)*, Kuala Lumpur, Malaysia, May 2016, pp. 1–6.

[2] A. de Jesus Torres, L. Sanguinetti, and E. Björnson, "Electromagnetic interference in RIS-aided communications," *IEEE Wireless Commun. Lett.*, vol. 11, no. 4, pp. 668–672, Apr. 2022.

[3] C.-J. Ku, L.-H. Shen, and K.-T. Feng, "Reconfigurable intelligent surface assisted interference mitigation for 6G full-duplex MIMO communication systems," in *Proc. IEEE Int. Symp. Person., Indoor, Mobile Radio Comm. (PIMRC)*, Kyoto, Japan, Sep. 2022, pp. 327–332.

[4] J. Ma, C. Li, and L. Du, "Interference suppression for RIS-assisted multicast communications," in *Proc. IEEE Int. Symp. Person., Indoor, Mobile Radio Comm. (PIMRC)*, Toronto, ON, Canada, Sep. 2023, pp. 1–6.

[5] L. Du, J. Ma, Q. Liang, C. Li, and Y. Tang, "Capacity characterization for reconfigurable intelligent surfaces assisted wireless communications with interferer," *IEEE Trans. Commun.*, vol. 70, pp. 1546–1558, Mar. 2022.

[6] J. Xu, L. Liu, and R. Zhang, "Multiuser MISO beamforming for simultaneous wireless information and power transfer," *IEEE Trans. Signal Proc.*, vol. 62, no. 18, pp. 4798–4810, Sept. 2014.

[7] M. Fu, Y. Zhou, and Y. Shi, "Reconfigurable intelligent surface for interference alignment in MIMO device-to-device networks," in *Proc. IEEE Int. Conf. Commun.*, Montreal, QC, Canada, Jun. 2021, pp. 1–6.

[8] Q. Li, M. El-Hajjar, I. Hemadeh, D. Jagyasi, A. Shojaeifard, and L. Hanzo, "Performance analysis of active RIS-aided systems in the face of imperfect CSI and phase shift noise," *IEEE Trans. Veh. Technol.*, vol. 72, no. 6, pp. 8140–8145, Jun. 2023.

[9] Q. Li, M. El-Hajjar, I. Hemadeh, D. Jagyasi, A. Shojaeifard, and L. Hanzo, "Achievable rate analysis of the STAR-RIS-aided NOMA uplink in the face of imperfect CSI and hardware impairments," *IEEE Trans. Commun.*, vol. 71, no. 10, pp. 6100–6114, Oct. 2023.

[10] Z. Zou, X. Wei, D. Saha, A. Dutta, and G. Hellbourg, "SCISRS: Signal cancellation using intelligent surfaces for radio astronomy services," in *Proc. IEEE GLOBECOM*, Rio de Janeiro, Brazil, Dec. 2022, pp. 4238–4243.

[11] X. Wei, A. Gupta, A. Dutta, D. Saha, and G. Hellbourg, "RIS for signal cancellation in 3D," in *Proc. IEEE Int. Symp. Dynamic Spectrum Access Netw. (DySPAN)*, Washington, DC, USA, May 2024, pp. 412–419.

[12] K. Zhong, J. Hu, H. Li, R. Wang, D. An, et al. "RIS-aided beamforming design for MIMO systems via unified manifold optimization," *IEEE Trans. Veh. Tech.*, vol. 74, pp. 674–685, Jan. 2025.

[13] M. Elsayed, A. S. Ibrahim, M. H. Ismail, and A. Samir, "Sum secrecy rate optimization in RIS-assisted ISAC systems: A manifold-based framework," *IEEE Wireless Commun. Lett.*, early access, pp. 1–1, 2025.

[14] S. Aghashahi, Z. Zeinalpour-Yazdi, A. Tadaion, M. B. Mashhadi, and A. Elzanaty, "MU-massive MIMO with multiple RISs: SINR maximization and asymptotic analysis," *IEEE Wireless Commun. Lett.*, vol. 12, no. 6, pp. 997–1001, Jun. 2023.

[15] J. Xu, W. Xu, and C. Yuen, "On performance of distributed RIS-aided communication in random networks," *IEEE Trans. Wireless Commun.*, vol. 23, no. 12, pp. 18254–18270, Dec. 2024.

[16] S. Naderi, D. A. Pados, G. Sklivanitis, E. S. Bentley, J. Suprenant, and M. J. Medley, "Self-optimizing near and far-field MIMO transmit waveforms," *IEEE J. Sel. Areas Comm.*, vol. 42, pp. 1673–1683, Jun. 2024.

[17] L. Wu, "Autonomous interference-avoiding machine-to-machine communications," *Nature Review Electr. Eng.*, May 2024.

[18] P.-A. Absil, R. Mahony, and R. Sepulchre, *Optimization Algorithms on Matrix Manifolds*, Princeton, NJ, USA: Princeton Univ. Press, 2008.

[19] Y. Liu, X. Liu, X. Mu, T. Hou, J. Xu, M. Di Renzo, and N. Al-Dhahir, "Reconfigurable intelligent surfaces: Principles and opportunities," *IEEE Commun. Surveys Tuts.*, vol. 23, no. 3, pp. 1546–1577, May 2021.

[20] R. A. Horn and C. R. Johnson, *Matrix Analysis*, Cambridge Un., 2012.

[21] N. Boumal, *An Introduction to Optimization on Smooth Manifolds*, Cambridge Un., 2023.

[22] S. Abeywickrama, R. Zhang, Q. Wu, and C. Yuen, "Intelligent reflecting surface: Practical phase shift model and beamforming optimization," *IEEE Trans. Commun.*, vol. 68, no. 9, pp. 5849–5863, Sep. 2020.

[23] E. Shtaiwi, H. Zhang, S. Vishwanath, M. Youssef, A. Abdelhadi, and Z. Han, "Channel estimation approach for RIS-assisted MIMO systems," *IEEE Trans. Cogn. Commun. Netw.*, vol. 7, no. 2, pp. 452–465, Jun. 2021.